



Sorption of bile salts from aqueous solutions by MCM-41 silica with chemically immobilized steroid groups

Nadiia V. Roik¹ · Lyudmila A. Belyakova¹ · Marina O. Dziazko¹

Received: 18 February 2022 / Accepted: 8 October 2022 / Published online: 7 November 2022
© King Abdulaziz City for Science and Technology 2022

Abstract

Mesoporous silicas of MCM-41 type with surface 3-aminopropyl and steroid groups were prepared by one-pot sol–gel synthesis in the presence of template. Structural parameters of synthesized materials were estimated using low-temperature nitrogen adsorption–desorption and X-ray diffraction analysis. It was found that introduction of cholic acid as co-template or its triethoxysilyl derivative as structure-forming agent in sol–gel synthetic mixture has positive impact on formation of hexagonally ordered mesoporous structure of MCM-41-type silicas and results in increase of surface area and narrowing of pores. The efficiency of synthesized silica materials in sorption removal of sodium cholate and taurocholate was studied from phosphate buffer solutions in dependence of duration of contact, solution pH, and adsorbate equilibrium concentration. It was found that maximal values of bile salts sorption are reached at pH ~ 5 for sodium cholate and at pH ~ 2 for sodium taurocholate after several hours of contact. Analysis of experimental sorption isotherms by the Langmuir, Freundlich, Redlich–Peterson, and BET models evidences multilayer character of bile salts sorption on MSNs. Noticeable increase of sodium cholate and taurocholate equilibrium sorption on silica material with chemically immobilized steroid groups in the region of small equilibrium concentrations at pH 5 as well as improved sorption ability at high equilibrium concentrations at pH 5 and pH 7 in comparison with parent aminosilica proves its potential efficiency in hypercholesterolemia diagnostics and treatment.

Keywords MCM-41 · Sol–gel synthesis · Bile acids · Sorption

Introduction

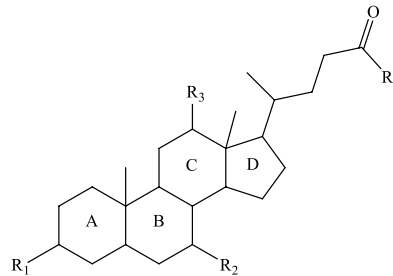
Bile acids (BAs) play the important role in human organism as biological surfactants for dietary fats and oil solubilization and transport. Primary bile acids, cholic (CA) and chenodeoxycholic (CDCA), which are formed in the result of sequence of enzymatic reactions occurring mainly in the liver, belong to the immediate products of cholesterol degradation. Whereas, secondary BAs, deoxycholic (DCA) and lithocholic (LCA), are produced at bacterial actions in the colon. In humans, primary as well as secondary BAs are conjugated to glycine or taurine (Scheme 1). BAs transport in the small bowel and undergo almost complete reabsorption in the distal ileum with subsequent reuptake from portal blood by the liver (Hofmann 2009; Watkins and Klaassen 2010; Dawson and Karpen 2015). Enterohepatic circulation

of BAs affects cholesterol metabolism and plays crucial role in pathogenesis of atherosclerosis (Hageman et al. 2010; Meissner et al. 2013; Bergheanu et al. 2017). Therefore, precise control of BAs' level in human biological systems and development of strategies for cholesterol excretion in the form of neutral sterols or BAs has noticeable importance in treatment of hypercholesterolemia.

Regulation of the cholesterol level in human organism can be achieved by removal of BAs excess from the gastrointestinal tract with enterosorbents. For this purpose, oral non-absorbable anion-exchange resins, such as Cholestyramine, Colestipol, and Colesevelam, are used in clinical practice for last decades (Cashin-Hemphill et al. 1991; Watts et al. 1992; Insull 2006). They reduce low-density lipoprotein cholesterol level due to binding of BAs, prevention their reabsorption in the intestine, and subsequent excretion in the feces. The most common adverse effects caused by BAs sequestrants are limited to the gastrointestinal tract (constipation, stomach pain, gas, nausea, and vomiting) and require the dose reduction. However, taking into account the low binding capacity of Cholestyramine, Colestipol,

✉ Nadiia V. Roik
roik_nadya@ukr.net

¹ Chuiko Institute of Surface Chemistry of NAS of Ukraine,
17 General Naumov Str., Kiev 03164, Ukraine

Scheme 1 Chemical structure of bile acids


Bile acid	R ₁	R ₂	R ₃	R ₄
CA	OH	OH	OH	OH
CDCA	OH(α)	OH(α)	H	OH
DCA	OH	H	OH	OH
UDCA	OH(α)	OH(β)	H	OH
LCA	OH	H	H	OH
GCA	OH	OH	OH	NHCH ₂ COO ⁻
TCA	OH	OH	OH	NHCH ₂ CH ₂ SO ₃ ⁻

and Colesevelam, which produce a reduction in low-density lipoprotein cholesterol of 18–25% (Reiner et al. 2011), this is extremely undesirable as leads to the decrease of therapeutic effect.

In the attempt to design highly efficient biocompatible sorbents for regulation of cholesterol level via removal of overproduced BAs from human blood or gastrointestinal tract, different functional materials, such as ion-exchange resins (Haratake et al. 1989; Chen et al. 2017; Sun et al. 2020), carbon materials (Krasopoulos et al. 1980; Sasaki et al. 1996; Yi et al. 2020), polysaccharides (Clas 1991; Nichifor et al. 2001; Kazlauske et al. 2014; Zhu et al. 2014; Shen et al. 2020) with improved structural characteristics, and surface layer properties, were studied over the past decades. Silica materials attract interest of scientists as promising candidates for design of medical sorbents because of large surface area and pore volume, easy surface functionalization, good biocompatibility, low toxicity, and high synthetic availability (Asefa and Tao 2012; Jaganathan and Godin 2012). However, sorption efficiency of hydroxylated silica in removal of bile acids from aqueous solutions decreases with pH rise and becomes insufficient in neutral and basic medium (Belyakova et al. 2006). Since pH varies in the range from 5.5 to 7.0 in the proximal small bowel and gradually rises up to 7.5 in the distal ileum, application of non-modified silica for binding of BAs in gastrointestinal tract is not reasonable.

Enhancement of BAs' sorption affinity can be achieved by creation of positively charged active centers (amino-propyl-, imidazolyl-, quaternary ammonium groups) or hydrophobization (trimethylsilyl groups) of silica surface (Belyakova et al. 2005, 2006). Promising results on removal of BAs from aqueous solutions were obtained for hybrid composite prepared by combination of chitosan, which is a natural polymer containing amino groups, with silica (Budnyak et al. 2019). Separation of amphiphilic molecules of individual and monosulfated conjugated BAs was realized

by reversed-phase partition thin-layer chromatography on octadecyl-bonded silica gel (Goto et al. 1978; Bloch and Watkins 1978; Raedsch et al. 1979). Molecularly imprinted silica for neutral sterols and BAs sorption as well as their selective recognition was obtained by introduction of estrone molecules into the imprinting matrix in the process of non-hydrolytic sol–gel synthesis with dimethylsulfoxide and acetic anhydride (Strand et al. 2012). Substantial improvement of silica sorption ability towards cholic acid was attained for silica with hydrophilic–hydrophobic mosaic structure designed by post-synthetic imprinting approach (Belyakova and Besarab 2007).

In the present study, mesoporous aminosilica nanoparticles (MSNs) of MCM-41 type with chemically immobilized BA-containing functional groups were prepared by template-assisted sol–gel condensation of structure-forming silanes. It is known that BAs are able to form self-assembled structures in the aqueous solutions due to the cooperative interactions (Carey and Small 1972; Roda et al. 1983). It was expected that sorption performance towards bile acids will be enhanced due to introduction of steroid groups into the surface layer of silica sorbent possessing high surface area, tunable pore diameter, and large pore volume. To elucidate contribution of BA-containing functional groups in sorption process, removal of bile salts (BSs), sodium cholate (NaC), and taurocholate (NaTC), was studied from aqueous solutions in dependence of duration of contact, solution pH, and adsorbate equilibrium concentration.

Experimental

Materials

Tetraethyl orthosilicate (TEOS) and (3-aminopropyl)triethoxysilane (APTES) (both from “Merck”, purity $\geq 99\%$), cholic acid (from “Fluka”, purity $\geq 99\%$),

cetyltrimethylammonium bromide (CTAB) (from “Merck”, purity $\geq 97\%$), and aqueous ammonia 25% (from “Reakhim”, analytical grade) were used in sol–gel and silane synthesis without preliminary purification. 1,1'-Carbonyldiimidazole (CDI) (from “Merck”, $\geq 98\%$) was employed as coupling agent as received. *N,N'*-Dimethylformamide (DMF) (from “Reakhim”, analytical grade) was dried prior usage in silane synthesis by stirring over activated molecular sieves (4 Å) at 293 K for 72 h. Hydrochloric acid 37% and ethanol 96% (both from “Reakhim”, chemical grade) were used in template extraction procedure without preliminary purification. Sodium cholate and taurocholate (both from “Frontier Scientific”, purity $\geq 98\%$) were used in sorption studies as received. Disubstituted sodium phosphate, monosubstituted potassium phosphate, and phosphoric acid (all from “Reakhim”, analytical grade) were used in phosphate buffers preparation without preliminary purification. Sulfuric acid 98% (from “Reakhim”, chemical grade) was employed for spectrophotometric determination of BSs without preliminary purification.

Template-assisted sol–gel synthesis of MSNs

Silica materials with hexagonally ordered mesoporous structure were synthesized by base-catalyzed sol–gel condensation of silica source in the presence of micelles of structure-directing agent (Grun et al. 1997). In the case of parent 1-MSN synthesis, weighted amount of CTAB was dissolved in distilled water. After that, 25% aqueous ammonia was poured into the surfactant solution and silanes mixture (TEOS and APTES) was slowly added under continuous stirring at 293 K (Table 1). The resultant reaction slurry was transferred into the polypropylene bottle, closed and allowed to age at 373 K without stirring for 24 h. Finally, the vacuum filtration of dispersion on Bunsen flask with Schott filter (pores 16 nm) was realized. The separated product of templated sol–gel synthesis was rinsed with deionized water and dried in air at 373 K for 2 h. Synthesis of 2-MSN with incorporated BA moieties was carried out by the same procedure using micellar system consisting of CTAB and CA as

template (Table 1). Whereas, 3-MSN with chemically immobilized steroid groups was obtained by sol–gel condensations of silanes mixture (TEOS, APTES, and CA-silane solution in DMF) in the presence of CTAB as template (Table 1).

CA-silane was synthesized by covalent attachment of highly reactive triethoxysilyl groups to CA through carbamate linkage formation between bile acid and APTES with CDI participation. Briefly, the batch of CA (0.004 mol) was placed into the flask with DMF (4 ml), dissolved, and treated with solution of CDI (0.0041 mol) in DMF (5 ml). Activation of CA carboxylic groups was achieved by stirring the reaction mixture at 293 K for 2 h. Then, APTES (0.004 mol) was added into the flask to link with activated CA. The solution was stirred at 293 K for 20 h and used in sol–gel synthesis of corresponding 3-MSN.

The molecules of template (CTAB) and co-template (CA) were removed from the pore channels of silica materials by extraction. For this, the batch of the as-synthesized material (1 g) was stirred with a solution of hydrochloric acid (8 ml) and ethanol (92 ml) at 298 K for 24 h. After separation of silica particles from solution by vacuum filtration of dispersion on Bunsen flask with Schott filter (pores 16 nm), the extraction procedure was repeated two more times. The resulting mesoporous silica was filtered, washed with deionized water until the absence of halogen ions (negative probe with silver nitrate) and BA (negative probe with concentrated sulfuric acid) in filtrate, and dried in the air at 373 K for 5 h.

For clarity, structure of surface layer of synthesized MCM-41-type silica materials is represented in Table 1.

Characterization of MSNs

Analysis of pore structure of synthesized MSNs was realized by low-temperature adsorption–desorption of nitrogen at 77 K with a Kelvin-1042 Sorptometer (Costech International, Italy). Prior to the analysis, MSNs samples were outgassed under vacuum at 413 K for 20 h. Nitrogen adsorption–desorption isotherms were measured over the region of relative pressures from 0.06 to 0.99 in increment of 0.015. The specific surface area S_{BET} was

Table 1 Molar composition of the reaction mixture and structure of surface layer of MSNs

Silica	Molar composition of the reaction mixture	Structure of surface groups	Content of surface groups	
			(mmol·g ⁻¹)	(μmol·m ⁻²)
1-MSN	0.096 TEOS: 0.004 APTES: 0.012 CTAB: 0.54 NH ₄ OH: 14.4 H ₂ O	≡SiOH –(CH ₂) ₃ NH ₂	0.28	0.54
2-MSN	0.096 TEOS: 0.004 APTES: 0.012 CTAB: 0.004 CA: 0.54 NH ₄ OH: 14.4 H ₂ O	≡SiOH –(CH ₂) ₃ NH ₂	0.25	0.45
3-MSN	0.096 TEOS: 0.004 CA-silane: 0.012 CTAB: 0.54 NH ₄ OH: 14.4 H ₂ O	≡SiOH –(CH ₂) ₃ NH ₂ –(CH ₂) ₃ NHCOCA	0.08 0.35	0.11 0.47

determined from the adsorption branch of isotherm by Brunauer–Emmett–Teller (BET) method (Brunauer et al. 1938). The pore size distribution was obtained from the adsorption branch of isotherm by non-local density functional theory (NLDFT) analysis assuming cylindrical pore structure of silica materials (Neimark et al. 1998). The total pore volume V_p of MSNs was calculated from the amount of adsorbed nitrogen at a relative pressure equal to 0.99 [Gregg and Sing 1913].

Powder X-ray diffraction patterns were obtained using a diffractometer DRON-4-02 (Burevestnik, Russia) with monochromatic $\text{CuK}\alpha$ emission ($\lambda = 0.15418$ nm) and nickel filter. The interplanar distance d was evaluated from the diffraction peak from (100) plane by the Bragg equation (Bragg 1913). The unit cell parameter a was calculated according to the equation represented in (Fenelonov et al. 1999). The diameter of cylindrical pores D was estimated by equation (Kruk et al. 1997)

$$D = cd \sqrt{\frac{\rho V_p}{1 + \rho V_p}}, \quad (1)$$

where V_p is the pore volume obtained from the results of low-temperature adsorption–desorption of nitrogen by the t-plot method; c is the constant predetermined by the pore shape and expressed as $c = \sqrt{\frac{8}{\sqrt{3}\pi}}$ for pores modeled as hexagonal prisms; d is the interplanar distance; ρ is the density of the pore walls that is equal to 2.2 g/cm (Kruk et al. 1997).

The thickness of the pore wall B was calculated as the difference between unit cell parameter a and diameter of cylindrical pores D by the equation

$$B = a - D. \quad (2)$$

The transmission electron microscopy (TEM) studies of MSNs were carried out on a JEOL JEM-100CXII electron microscope (JEOL Ltd., Japan) at 200 kV. Carbon-coated copper grids were used as silica holders.

Chemical structure of synthesized silica materials was confirmed by IR spectra recorded on a Thermo Nicolet NEXUS FT-IR spectrophotometer (Nicolet, USA) in the range from 4000 to 400 cm^{-1} with a resolution of 2 cm^{-1} .

The content of 3-aminopropyl groups chemically immobilized on silica surface was estimated by the potentiometric titration with 0.1 M HCl.

The amount of CA-containing groups introduced into the silica in the process of sol–gel synthesis was determined by acid–base hydrolysis of 3-MSN and subsequent analysis of colored complex of hydrolyzate with concentrated sulfuric acid (Ripatti et al. 1969) using a spectrophotometer Specord M-40 (Carl Zeiss, Jena). For this, the batch

of 3-MSN silica (0.05 g) was placed in a reactor with a reflux condenser, suspended in a small amount of 1 M H_2SO_4 (10 ml), and refluxed at 373 K for 2 h. After that the suspension was cooled to room temperature and neutralized to $\text{pH} \sim 7$ with NaOH solution. Resulting suspension was mixed with 5 M NaOH solution (7 ml), refluxed at 373 K for 2 h, and cooled to room temperature. Content of CA in analyzed solution was determined by color reaction with concentrated sulfuric acid. For this, solution containing bile acid (5 ml) was placed in 50 ml glass beaker and concentrated sulfuric acid (5 ml) was carefully added. Prepared mixture was heated at 333 K in temperature-controlled water bath for 1 h, cooled to room temperature, and analyzed with a spectrophotometer Specord M-40 using calibration curve measured at $\lambda = 389$ nm in the range of concentrations 0–0.5 mmol/l.

Sorption of BSs on MSNs

UV–Vis spectra of BSs colored complexes with concentrated sulfuric acid were recorded in 200–600 nm spectral range with a Specord M-40. Quartz cells with 5 and 10 mm path length were used for NaC and NaTC phosphate buffer solutions (PBS), correspondingly. All sorption studies were made with temperature-controlled water bath. pH of solutions were measured by an Ionometer I-120.1 that was calibrated for optimal precision using standard buffer solutions with pH 1.68 and 6.86.

The kinetic sorption behavior of BSs on MSNs was studied to evaluate the time required for equilibrium attainment. For this, series of MSNs batches (0.02 g) were placed in 50 ml glass beakers and 0.3 mmol/l solutions of BSs (10 ml) in PBS with pH 5 were added. Prepared suspensions were shaken at 297 K for different contact time and supernatant solutions were separated by filtering through a 0.22 μm PVDF syringe filter. Obtained aliquots (5 ml) were placed in 50 ml glass beakers and equal volumes of concentrated sulfuric acid (5 ml) were carefully added. Prepared mixtures were heated at 333 K in temperature-controlled water bath for 1 h, cooled to room temperature, and analyzed with a spectrophotometer Specord M-40. Concentration of BSs was estimated from the value of optical density of absorption band at $\lambda = 389$ nm. The amount of NaC or NaTC sorbed on MSNs surface at time t was calculated by the equation

$$A_t = \frac{(C_o - C_t) \cdot V}{m}, \quad (3)$$

where A_t is the content of BS sorbed on MSNs surface at time t , mmol/g; C_o and C_t are the concentrations of BS at

initial moment and at time t , correspondingly, mmol/l; V is the volume of solution, l; m is the weight of sorbent used, g.

Sorption of NaC or NaTC on synthesized mesoporous silica materials in dependence of pH was carried out from 0.18 mmol/l solutions of BSs in PBS. Briefly, batches of silicas (0.02 g) were placed in 50 ml glass beakers and solutions of BSs in PBSs (10 ml) with predetermined pH in the range from 1.0 to 8.0 were added. Prepared suspensions were shaken at 297 K for equilibrium attainment. Supernatant solutions were separated by filtering through a 0.22 μm PVDF syringe filter. Obtained aliquots (5 ml) were placed in 50 ml glass beakers and equal volumes of concentrated sulfuric acid (5 ml) were carefully added. Prepared mixtures were heated at 333 K in temperature-controlled water bath for 1 h, cooled to room temperature, and analyzed with a spectrophotometer Specord M-40. Concentration of BSs was estimated from the value of optical density of absorption band at $\lambda = 389$ nm. The amount of NaC or NaTC sorbed on silica surface at equilibrium was calculated using calibration curves plotted for each pH value by the equation

$$A = \frac{(C_o - C_{eq}) \cdot V}{m}, \quad (4)$$

where A is the content of BS sorbed on silica surface at equilibrium, mmol/g; C_o and C_{eq} are the concentrations of BS at initial moment and at equilibrium, correspondingly, mmol/l; V is the volume of solution, l; m is the weight of sorbent used, g.

Equilibrium sorption of BSs on synthesized MSNs was studied from 0.06 to 0.3 mmol/l solutions in PBS with pH 5.0 and 7.4. The amount of BSs sorbed on silica surface at equilibrium was calculated as described above (Eq. 4).

Results and discussion

Micelles of cationic surfactant play the role of structure-directing agent in sol–gel synthesis assisting formation of ordered pore system typical for MCM-41 silica. Solubilization of amphiphilic additives like bile acids by surfactant micelles causes changes in composition, critical micelle concentration, and geometry configuration of supramolecular aggregates (Jana and Moulik 1991; Swanson-Vethamuthu et al. 1996; Padasala et al. 2016). As a result, alteration in structure of silica material obtained by template-assisted sol–gel synthesis can be expected. Molecules of CA introduced in surfactant solution integrate into the micelles of CTAB due to the electrostatic and hydrophobic interactions. Whereas, CA-silane moieties able for simultaneous interaction with micellar and extra-micellar environment at sol–gel synthesis. Along with incorporation inside micelles of CTAB, they participate in sol–gel condensation reaction with structure-forming silanes proceeding around template aggregates. The influence of CA as structure-directing and CA-silane as structure-forming agent on MSNs characteristics was studied by low-temperature nitrogen adsorption–desorption and X-ray diffraction analysis.

Isotherms and pore size distributions of synthesized MSNs are shown in Figs. 1 and 2, correspondingly. It can be seen that the profile of nitrogen adsorption–desorption isotherm on 1-MSN belongs to the type II with hysteresis loop of the type H3 according to the IUPAC classification (Fig. 1). Introduction of CA and CA-silane in sol–gel synthesis results in 2-MSN and 3-MSN, correspondingly, for which adsorption–desorption isotherms of the type IV with hysteresis loop of the type H3 are registered (Fig. 1). For this type of isotherms, a linear increase in nitrogen

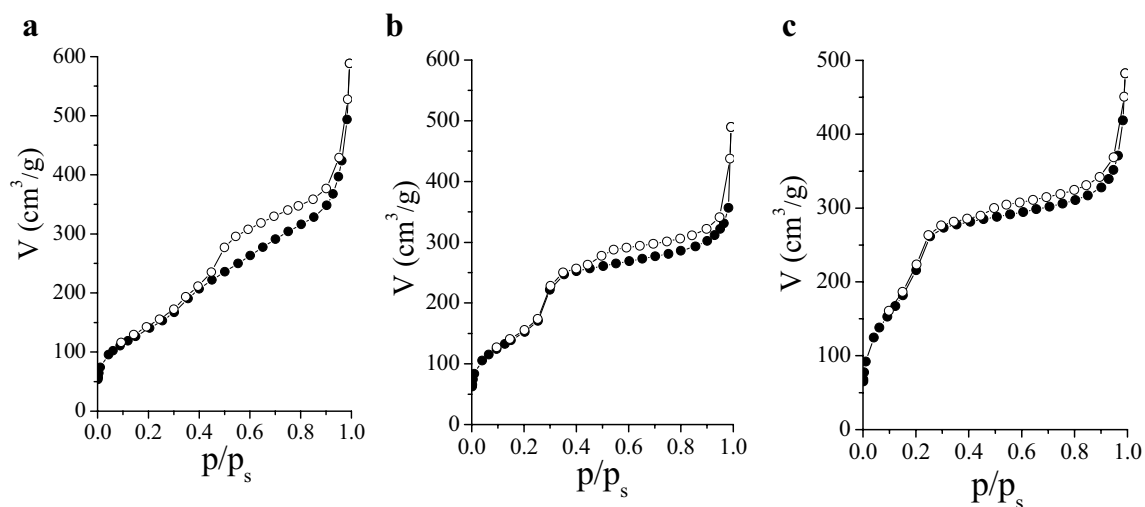


Fig. 1 Isotherm of low-temperature nitrogen adsorption–desorption on 1-MSN (a), 2-MSN (b), and 3-MSN (c)

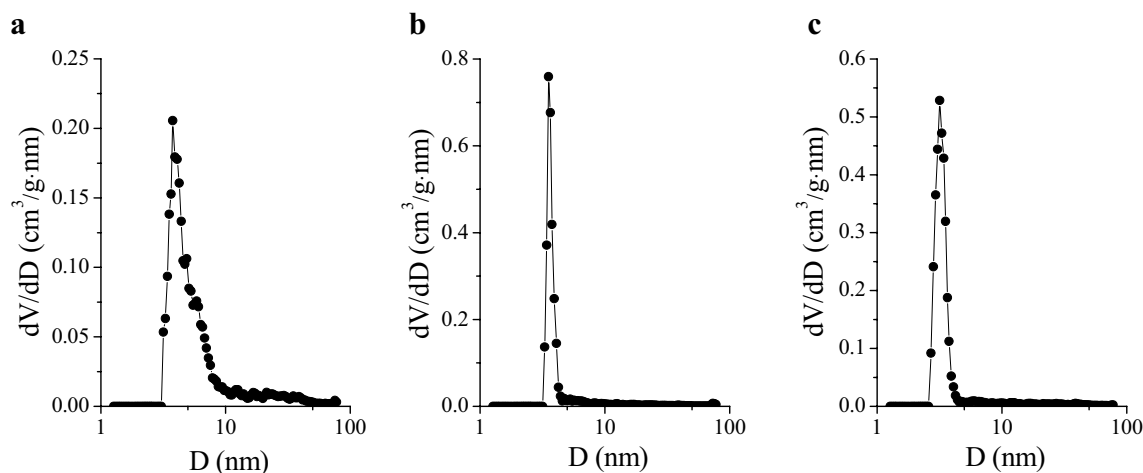


Fig. 2 Pore size distribution in 1-MSN (a), 2-MSN (b), and 3-MSN (c)

adsorption is followed by its sharp rise at relative pressures from 0.25 to 0.35 due to capillary condensation within uniform mesopores. Obviously, transformation of isotherms profiles confirms improvement of hexagonally arranged mesoporous structure typical for MCM-41 due to addition of amphiphilic substances in sol–gel synthesis. As it can be seen from Fig. 1, isotherms of synthesized materials exhibit adsorption hysteresis, which is appeared due to capillary condensation and explained by the difference in the curvature of the meniscus on adsorption and desorption process. The distinct step on the desorption branch of isotherms at hysteresis loop closure ($p/p_o \sim 0.42$) is generated by narrowing of pore entrances and removal of adsorbate from the pores of silica materials via the cavitation process (Van Der Voort et al. 2002; Thommes et al. 2006; Lai et al. 2020). In other words, evaporation of adsorbate does not proceed at the relative pressure corresponding to the size of cylindrical mesopores of synthesized materials and takes place at the critical pressure defined by the tensile strength effect. To get the valid information about mesoporous structure of synthesized materials, pore size distributions were calculated by applying NLDFT to the adsorption branch of isotherms (Van Der Voort et al. 2002; Thommes et al. 2006; Landers et al. 2013) (Fig. 2). According to the obtained results, uniform mesopores are prevailing in synthesized MSNs (Fig. 2). Along with reduction of hysteresis loop on

nitrogen adsorption–desorption isotherms, noticeable narrowing of pores in the range 1-MSN > 2-MSN > 3-MSN is observed (Figs. 1, 2, Table 2). Analysis of structural parameters of MSNs clearly indicates that introduction of CA as co-templating agent or CA-silane as structure-forming agent in sol–gel synthesis results in substantial increase of surface area and narrowing of pore diameters, which are more pronounced in the case of CA-silane. It can be supposed that narrowing of pore channels is generated by penetration of hydrophobic parts of CA-silane between chains of template micelles and drawing of silica matrix closure to the micelles core.

The X-ray diffraction patterns of synthesized MSNs are shown in Fig. 3. It can be seen that diffractogram of 1-MSN has only one low-intensity reflection from the (100) plane at 2θ equal to 2.25 deg (Fig. 3). This indicates some disruption of hexagonal arrangement of pore channels in 1-MSN. Introduction of CA as co-templating agent in sol–gel synthesis results in 2-MSN with improved hexagonally ordered mesoporous structure. Three well-resolved diffraction peaks assigned to the (100), (110), and (200) planes are registered on the diffractogram of 2-MSN (Fig. 3). The position of (100) reflex is shifted to low-angle region and registered at 2.15 deg, whereas its intensity is increased almost double as compared to 1-MSN (Fig. 3). Therefore, CA as co-templating agent causes increase of interplanar distance (Table 2). For 3-MSN obtained by use of CA-silane as silica source,

Table 2 Structural parameters of mesoporous silica materials

Silica	Low-temperature nitrogen adsorption–desorption			X-ray diffraction analysis			
	S_{BET} (m ² /g)	V (cm ³ /g)	D (nm)	d_{100} (nm)	a (nm)	D (nm)	B (nm)
1-MSN	515	0.91	3.78	3.93	4.53	3.89	0.64
2-MSN	550	0.76	3.54	4.11	4.75	3.94	0.81
3-MSN	740	0.75	3.18	3.93	4.53	3.76	0.77

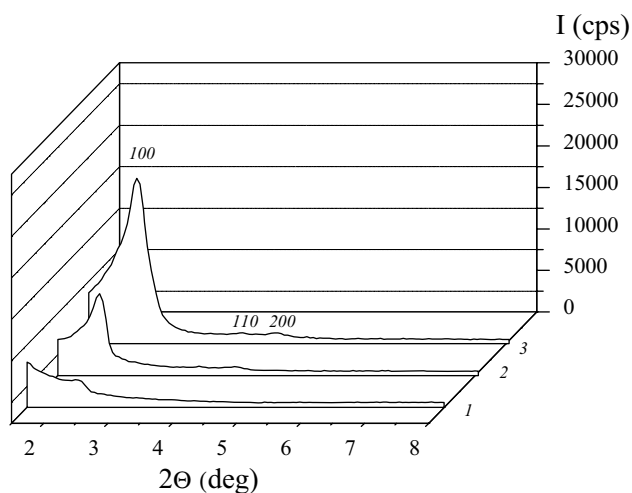
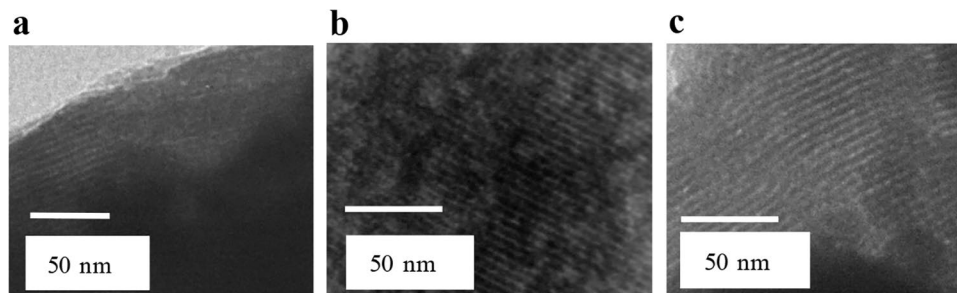


Fig. 3 X-ray diffraction patterns of 1-MSN (curve 1), 2-MSN (curve 2), and 3-MSN (curve 3)

the X-ray diffraction reflex from the (100) plane retains the same position as for parent 1-MSN and registered at 2θ equal to 2.25 deg (Fig. 3). As can be clearly seen from Fig. 3, intensities of all reflections including higher angle ones are noticeably enhanced. This fact indicates that organosilica with chemically immobilized CA-containing groups have more uniform hexagonally ordered mesoporous structure in comparison with parent amino silica and synthesized in the presence of CA one. The results of X-ray diffraction studies confirm that CA additive as component of structure-directing micelles and CA-containing silane as structure-forming agent have positive impact on formation of hexagonally ordered mesoporous structure of MCM-41-type silicas. This fact can be explained by tight interactions arising between hydrophobic parts of introduced compounds and long alkyl chains of cationic surfactant on the one side and between hydrophilic groups of additives and growing anionic oligomers of orthosilicic acid on the other side. Synthesized MSNs have hexagonally arranged porous structure with relatively narrow distribution of cylindrical channels suitable for biologically active compounds sorption.

Fig. 4 TEM images of 1-MSN (a), 2-MSN (b), and 3-MSN (c)



To confirm formation of uniformly distributed cylindrical channels suitable for biologically active compounds sorption, visualization of structure by TEM analysis was carried out. As can be seen in Fig. 4, synthesized materials have hexagonally arranged cylindrical mesopores, entrances to which are oriented outside of particles that provide accessibility of functional groups for sorbate molecules.

Chemical immobilization of steroid groups in surface layer of 3-MSN was confirmed by FT-IR spectral (Fig. 5) and quantitative chemical analysis (Table 1). In the IR spectrum of MSN-3, there are absorption bands in the regions 2800–3000 and 1300–1500 cm^{-1} attributed to the valence and deformation vibrations, correspondingly, of the C–H bonds in the methyl radicals of chemically immobilized groups (Fig. 5). Moreover, characteristic absorption band caused by deformation vibrations of the N–H bond in the amide group is registered at 1554 cm^{-1} (Fig. 5). IR identification of absorption band of valence vibrations of the C=O bond in the amide linkage which is expected nearby 1700 cm^{-1} is complicated because of its overlapping with strong signal attributed to the deformation vibrations of the O–H bond in the adsorbed water molecules.

Equilibrium conditions for synthesized MSNs are reached from 2 to 4 h of contact with BSs solutions (Fig. 6, 7). To define the most appropriate model for estimation of kinetic rate constants and amounts of BSs sorbed at equilibrium

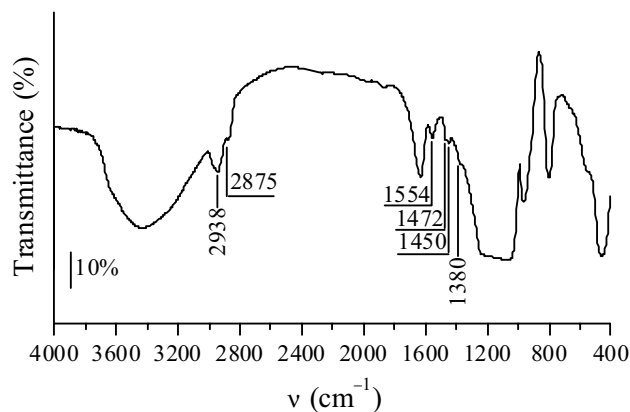


Fig. 5 IR spectrum of 3-MSN

Fig. 6 Kinetic curves of NaC (a) and NaTC (b) sorption on 1-MSN (curve 1), 2-MSN (curve 2), and 3-MSN (curve 3) from PBS with pH 5.0 at 297 K (batch of sorbent – 0.02 g, initial concentration of BS – 0.3 mmol/l)

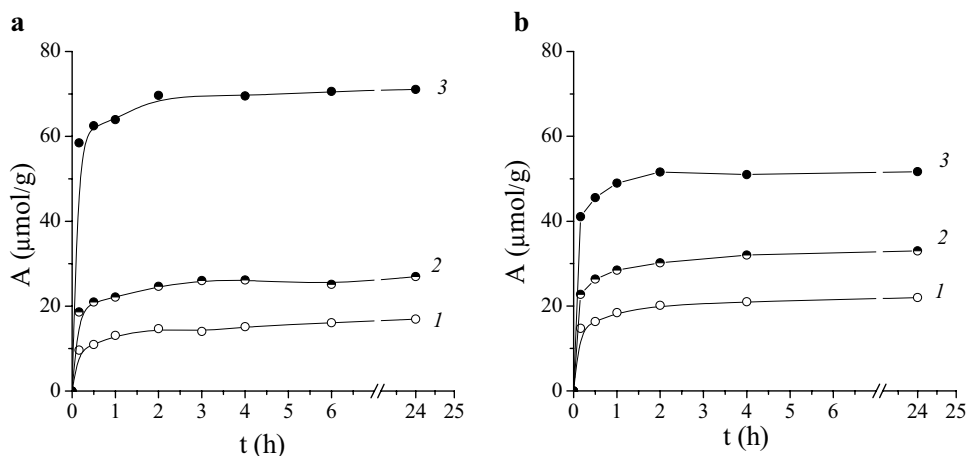
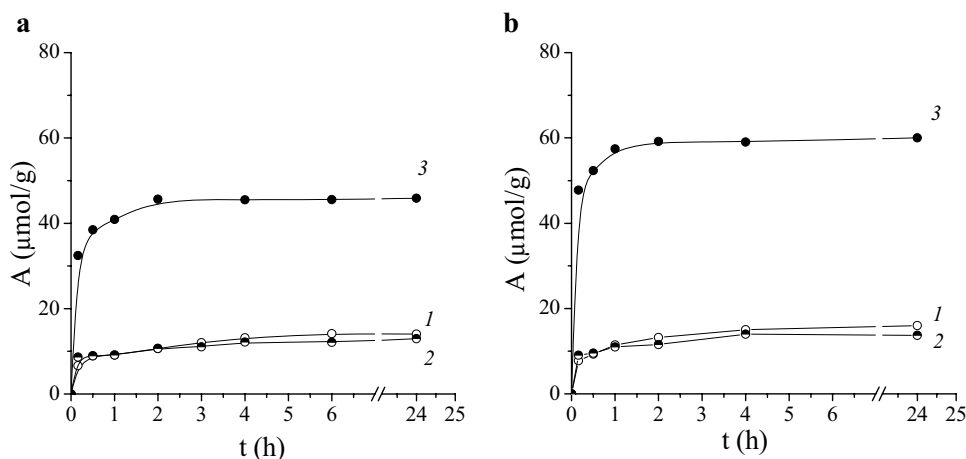


Fig. 7 Kinetic curves of NaC (a) and NaTC (b) sorption on 1-MSN (curve 1), 2-MSN (curve 2), and 3-MSN (curve 3) from PBS with pH 7.4 at 297 K (batch of sorbent – 0.02 g, initial concentration of BS – 0.3 mmol/l)



attainment, experimental kinetic data were analyzed by Lagergren and Ho-McKey equations of pseudo-first and pseudo-second order (Table 3), correspondingly. Obtained results prove that sorption of BSs on 1-MSN, 2-MSN, and 3-MSN from PBS with pH 5.0 and 7.4 follows the pseudo-second order kinetic model. Despite the fact that the high values of R^2 were obtained for NaC and NaTC sorption on MSNs by applying of both kinetic equation, in all cases, correlation coefficients for Ho-McKey linear plot exceed those for Lagergren (Table 3). Comparison of the kinetic sorption parameters demonstrates noticeable difference in A_{eq} values calculated by Lagergren and Ho-McKey equations. Pseudo-second-order kinetic model provides better agreement of calculated values of A_{eq} with the experimental data. It can be supposed that this discrepancy is generated by the necessity to specify the A_{eq} in the linear equation of the pseudo-first-order kinetic model. Analysis of kinetic parameters for BSs sorption on 1-MSN and 2-MSN indicates that introduction of CA as co-template in sol-gel synthesis in most cases results in substantial increase of kinetic rate constants. Obviously, improvement of mesoporous structure

hexagonal ordering of 2-MSN has positive impact on kinetic sorption parameters of silica sorbent.

Efficiency of BSs sorption removal by MSNs is predetermined by the protolytic state of adsorbate and adsorbent ionogenic groups. Therefore, in the present work, the effect of pH on the distribution of protolytic forms and adsorbate-adsorbent interactions was studied. Obtained results can be useful in understanding the most favorable conditions for sorption removal of BSs by synthesized silica materials. The distributions of protolytic forms of BAs and surface functional groups of MSNs as a dependence of pH were generated for the parameter set chosen by the Curtipot program version 4.3.1.

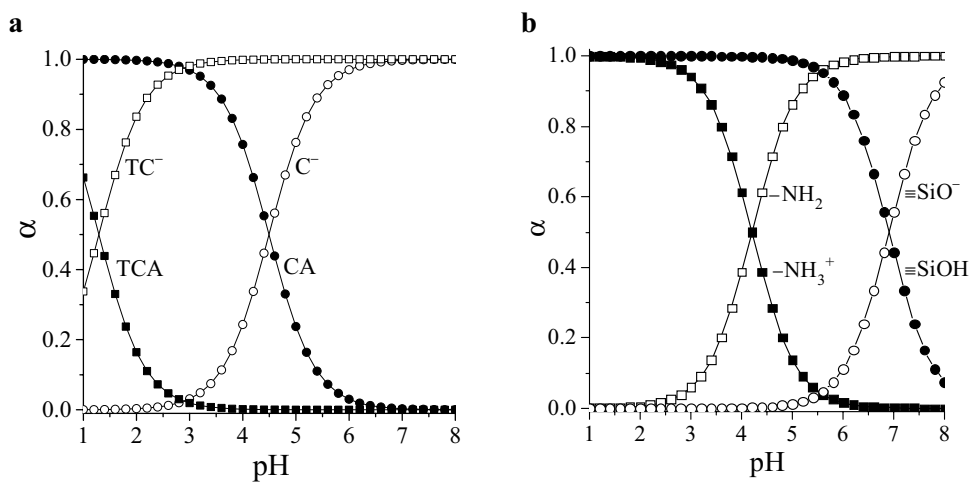
As it can be seen from the Fig. 8, CA exists in molecular form at pH below 4.6 ($pK_a = 4.6$), whereas dissociated form of TCA prevails over the entire studied pH range ($pK_a = 1.4$). Therefore, gradual increase of NaC sorption by 1-MSN and 2-MSN with pH rises from 1 up to 5 is mainly associated with hydrogen bonds formation between molecular form of BA and non-ionized silanol ($pK_a = 6.9$) as well as unprotonated 3-aminopropyl groups ($pK_a = 3.8$) of silica surface,

Table 3 Kinetic parameters for BSs sorption on MSNs from PBS with pH 5.0 and 7.4 at 297 K

Adsorption reaction model			Lagergren			Ho-McKay		
Equation			$\lg \left(\frac{A_{eq}}{A_{eq}-A_t} \right) = \frac{k_1}{2.303} t$			$\frac{1}{(A_{eq}-A_t)} = \frac{1}{A_{eq}} + k_2 t$		
Linear form of equation			$\lg (A_{eq} - A_t) = \lg A_{eq} - \frac{k_1}{2.303} t$			$\frac{t}{A_t} = \frac{1}{k_2 A_{eq}^2} + \frac{1}{A_{eq}} t$		
Kinetic parameters			k_1	A_{eq}	R^2	k_2	A_{eq}	R^2
NaC	pH 5.0	1-MSN	0.566	9.411	0.964	0.159	17.167	0.999
		2-MSN	0.395	6.024	0.904	0.195	27.100	0.999
		3-MSN	0.772	11.098	0.823	0.197	71.276	0.999
	pH 7.4	1-MSN	0.566	9.411	0.964	0.178	14.304	0.999
		2-MSN	0.395	6.024	0.904	0.212	13.115	0.999
		3-MSN	0.772	11.098	0.823	0.313	46.019	1
NaTC	pH 5.0	1-MSN	0.651	9.690	0.902	0.263	22.143	0.999
		2-MSN	0.719	13.806	0.915	0.213	33.179	0.999
		3-MSN	1.015	11.407	0.738	0.397	51.813	1
	pH 7.4	1-MSN	0.617	10.367	0.969	0.178	16.221	0.999
		2-MSN	0.729	7.401	0.821	0.389	13.818	0.999
		3-MSN	0.877	14.507	0.806	0.311	60.132	1

A_{eq} is the content of BS sorbed on MSNs at equilibrium, $\mu\text{mol/g}$; A_t is the content of BS sorbed on MSNs at time t , $\mu\text{mol/g}$; k_1 is the rate constants of Lagergren equation, min^{-1} ; k_2 is the rate constants of Ho-McKey equation, $\text{g}/\mu\text{mol}\cdot\text{min}$

Fig. 8 Distribution diagrams of protolytic forms of BAs (a) as well as surface silanol and 3-aminopropyl groups of silica materials (b) as a function of pH value

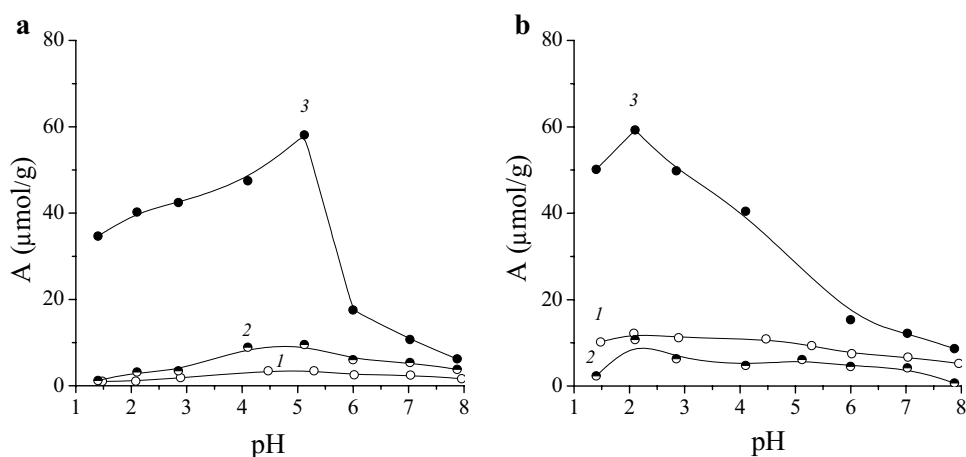


which appears at lower solution acidity (Figs. 8, 9). Accumulation of cholate anions in solution and ionized functional groups on silica surface which takes place at $\text{pH} > 5$ disfavors sorption process and results in decrease of NaC sorption removal (Fig. 9). Difference in protolytic properties of BSs causes noticeable changes in their sorption behavior. The highest values of NaTC sorption are achieved in acidic medium where process is driven by hydrogen bonds formation between anionic form of BA and non-ionized silanol as well as protonated 3-aminopropyl groups of MSNs (Fig. 8, 9). Slight suppression of 1-MSN and 2-MSN removal efficiency towards NaTC with pH rise is caused by electrostatic

repulsion between negatively charged adsorbate and ionized silanol as well as unprotonated 3-aminopropyl groups having unshared electron pair on the nitrogen atom (Fig. 8, 9).

Introduction of steroid groups in surface layer of silica sorbent leads to the substantial enhancement of sorption efficiency towards BSs. The amount of NaC or NaTC sorbed from 0.18 mmol/l solution of corresponding BS in PBS with pH 5.0 or 7.4 by silica materials with surface silanol and 3-aminopropyl groups is extremely low and does not exceed $11 \mu\text{mol/g}$. However, it is increased more than fivefold and reaches almost $60 \mu\text{mol/g}$ in the case of 3-MSN. Maximal values of BSs sorption removal

Fig. 9 Effect of pH on NaC (a) and NaTC (b) sorption by 1-MSN (curve 1), 2-MSN (curve 2), and 3-MSN (curve 3) from PBS at 297 K (batch of sorbent – 0.02 g, initial concentration of BS – 0.18 mmol/l)



are predetermined by the protolytic properties of corresponding BAs and achieved at pH ~ 5 for NaC and pH ~ 2 for NaTC (Fig. 8, 9). Consequently, substantial difference in sorption efficiency of synthesized silica materials is mainly attributed to the chemical immobilization of steroid groups.

Therefore, it is evident that solution pH exerts a significant influence on BSs sorption by MSNs. To get an idea of the potential advantages of silica with chemically immobilized steroid groups in sorption removal of BSs in the gastrointestinal tract, equilibrium sorption studies were carried out at pH level of small intestine (Reddy et al. 1980; Evans et al. 1988). It was expected that analysis of isotherms obtained at pH 5.0 and pH 7.4, where different protolytic forms of adsorbate and surface functional groups of adsorbent are present in suspension, will clarify the main driving forces of BSs sorption process on synthesized silica materials.

As it can be seen from Figs. 10 and 11, isotherms of BSs sorption by MSNs with surface silanol and 3-aminopropyl groups have similar profiles typical for weak adsorbate–adsorbent interactions in the region of small equilibrium concentration. The main contribution in sorption removal

of BSs by 1-MSN and 2-MSN at pH 5.0 belongs to the hydrogen-bond formation between molecular form of CA and non-ionized silanol as well as unprotonated 3-aminopropyl groups or anionic forms of CA or TCA and non-ionized silanol groups (Fig. 8). In addition, side hydroxyls of BSs may contribute in sorption process due to hydrogen-bond formation with surface groups of MSNs. It should be pointed out that interaction of cholate and taurocholate anions, which prevail in solution at pH 7.4, with ionized silanol as well as unprotonated 3-aminopropyl groups of silica surface is unfavorable. Therefore, sorption proceeds mainly due to hydrogen bonding of hydroxyl groups of BSs with functional groups of silica surface. In both cases, gradual rise of isotherms is observed at higher equilibrium concentrations of BSs in solution that may be related to the cooperative interactions of cholate and taurocholate anions with secondary adsorption sites formed on MSNs surface by adsorbate (Figs. 10, 11). In general, obtained experimental results indicate low sorption affinity of 1-MSN and 2-MSN to BSs (Figs. 10, 11).

Profiles of BSs sorption by 3-MSN at studied pH values differ substantially (Figs. 10, 11). Drastic enhancement of

Fig. 10 Isotherms of NaC (a) and NaTC (b) sorption by 1-MSN (curve 1), 2-MSN (curve 2), and 3-MSN (curve 3) from PBSs with pH 5.0 at 297 K (batch of sorbent – 0.02 g, initial concentration of BS – 0.06–0.3 mmol/l)

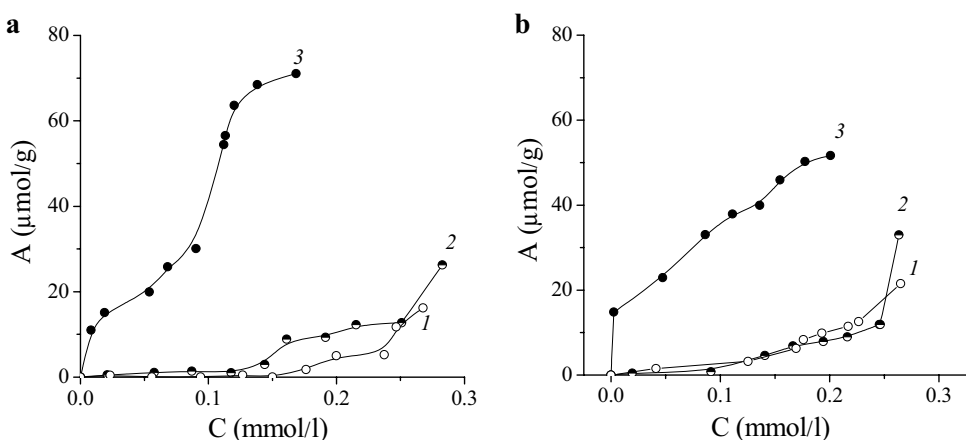
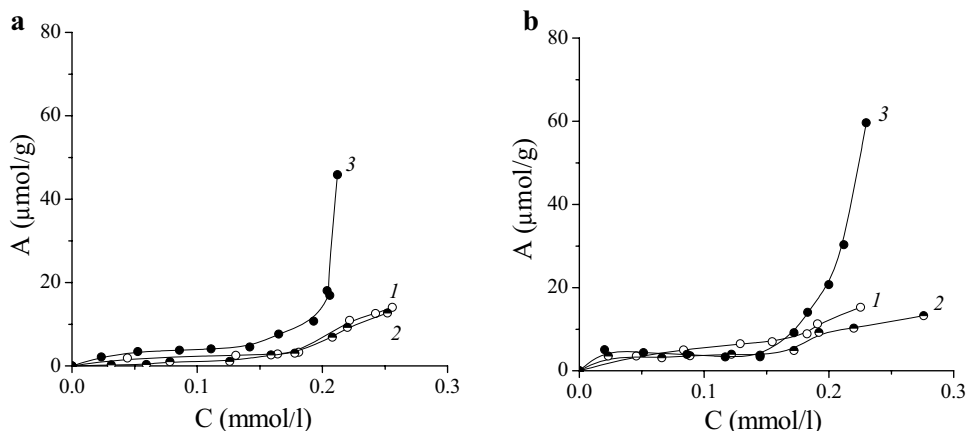


Fig. 11 Isotherms of NaC (a) and NaTC (b) sorption by 1-MSN (curve 1), 2-MSN (curve 2), and 3-MSN (curve 3) from PBSs with pH 7.4 at 297 K (batch of sorbent – 0.02 g, initial concentration of BS – 0.06 – 0.3 mmol/l)



NaC and NaTC sorption removal by 3-MSN from PBS with pH 5.0 begins at small equilibrium concentrations (Fig. 10). Obviously, chemically immobilized CA-containing functional groups facilitate interaction of silica surface with BSs. Contrariwise, negligible sorption of BSs by 3-MSN in the initial region of isotherm curves that is followed by sharp rise at higher equilibrium concentrations (> 0.2 mmol/l) is observed at pH 7.4 (Fig. 11). Therefore, isotherms of NaC and NaTC sorption by 3-MSN from PBS with pH 7.4 resemble that ones obtained for MSNs with surface silanol and 3-aminopropyl groups. This fact confirms arising of weak interaction between adsorbate and adsorbent in the region of small equilibrium concentration at pH 7.4.

To complete the analysis of equilibrium concentration effect on sorption removal of BSs by MSNs from PBS with pH 5.0 and pH 7.4, experimental sorption isotherms were described by the Langmuir, Freundlich, Redlich–Peterson, and BET models. For this, linear plot of isotherms in coordinates of the Langmuir and Freundlich equations or their non-linear regression analysis using the Redlich–Peterson and BET equations was carried out and obtained results are summarized in Tables 4, 5 and 6. Precise values of equilibrium sorption parameters were estimated from the best fitted isotherm model. The values of the correlation coefficients (R^2) of the linearized Langmuir and Freundlich equations are significantly lower compared to that ones obtained at non-linear modeling of experimental results with the Redlich–Peterson

Table 4 Parameters of BSs equilibrium sorption on MSNs calculated using the Langmuir and Freundlich models

Equilibrium sorption model			Langmuir			Freundlich		
Linear form of equation			$\frac{C_{eq}}{A_{eq}} = \frac{1}{K_L A_m} + \frac{C_{eq}}{A_m}$			$\lg A_{eq} = \lg K_F + \frac{1}{n} \lg C_{eq}$		
Sorption parameters			K_L	A_m	R^2	K_F	n	R^2
NaC	pH 5.0	1-MSN	3.608	0.171	0.483	47.098	0.505	0.646
		2-MSN	2.887	4.818	0.592	95.356	0.657	0.900
		3-MSN	3.961	165.016	0.460	205.362	1.518	0.930
	pH 7.4	1-MSN	1.567	13.092	0.301	39.784	0.897	0.784
		2-MSN	3.707	1.586	0.848	115.279	0.519	0.949
		3-MSN	1.250	37.707	0.221	72.872	0.947	0.807
NaTC	pH 5.0	1-MSN	2.186	12.366	0.703	85.517	0.751	0.943
		2-MSN	3.098	4.320	0.605	92.920	0.681	0.902
		3-MSN	31.569	54.407	0.953	70.261	3.717	0.962
	pH 7.4	1-MSN	1.049	62.112	0.306	40.163	1.212	0.941
		2-MSN	1.726	29.629	0.282	16.408	1.902	0.729
		3-MSN	1.096	45.829	0.117	52.369	1.240	0.606

A_{eq} is the amount of BS sorbed on silica surface, $\mu\text{mol/g}$; C_{eq} is the concentration of BS remaining in the solution after equilibrium attainment, mmol/l ; A_m is the amount of BS required to form monolayer on the sorbent surface, $\mu\text{mol/g}$; K_L is the Langmuir constant related to the affinity of the binding sites, μmol^{-1} ; K_F and n are the Freundlich constants that indicate the extent of surface heterogeneity, g^{-1} ; $1/n$ is the measure of sorption intensity, which can be between 0 and 1

Table 5 Parameters of BSs equilibrium sorption on MSNs calculated using the Redlich–Peterson model

Equilibrium sorption model			Redlich–Peterson				
Linear form of equation			$A_{eq} = \frac{K_R C_{eq}}{1 + a_R C_{eq}^\beta}$				
Sorption parameters			K_R	a_R	β	R^2	χ^2
NaC	pH 5.0	1-MSN	31.759	6.674×10^{-4}	1×10^{-12}	0.529	17.849
		2-MSN	65.475	0.157	1×10^{-14}	0.723	20.889
		3-MSN	1.262×10^5	273.554	4.207×10^{-15}	0.932	55.307
	pH 7.4	1-MSN	47.084	0.127	1×10^{-16}	0.705	12.656
		2-MSN	41.504	0.259	1×10^{-16}	0.695	7.583
		3-MSN	92.429	1×10^{-14}	1×10^{-8}	0.452	116.978
NaTC	pH 5.0	1-MSN	67.172	0.191	1×10^{-16}	0.790	12.258
		2-MSN	68.097	0.133	1×10^{-16}	0.536	55.490
		3-MSN	8.285	9.664	0.648	0.955	17.492
	pH 7.4	1-MSN	57.137	4.021×10^{-6}	4.1×10^{-9}	0.914	2.684
		2-MSN	54.975	0.296	2.344×10^{-16}	0.833	3.478
		3-MSN	146.606	0.204	1×10^{-16}	0.480	202.313

K_R and a_R are the Redlich–Peterson isotherm constants, l/g and l/mmol, correspondingly; β is the exponent that lies between 0 and 1 (sorption model follows the Langmuir model when β value is 1, while when β value is 0, the sorption model follows the Henry’s law)

Table 6 Parameters of BSs equilibrium sorption on MSNs calculated using the BET model

Equilibrium sorption model			Brunauer–Emmett–Teller				
Linear form of equation			$A_{eq} = \frac{A_m K_S C_{eq}}{(1 - K_L C_{eq})(1 - K_L C_{eq} + K_S C_{eq})}$				
Sorption parameters			K_S	K_L	A_m	R^2	χ^2
NaC	pH 5.0	1-MSN	0.089	3.787	8.706	0.999	0.003
		2-MSN	6.612	3.001	4.177	0.937	4.734
		3-MSN	192.704	5.684	15.896	0.932	2.031×10^{-4}
	pH 7.4	1-MSN	0.059	2.414	149.524	0.946	2.299
		2-MSN	0.045	2.536	158.079	0.972	0.699
		3-MSN	2.257	4.607	1.055	0.975	5.289
NaTC	pH 5.0	1-MSN	2.832	2.772	7.698	0.989	0.597
		2-MSN	151.123	3.617	1.543	0.958	4.995
		3-MSN	515.718	2.656	25.643	0.980	7.625
	pH 7.4	1-MSN	82.704	3.360	3.776	0.988	0.368
		2-MSN	143.723	2.757	3.330	0.892	2.248
		3-MSN	0.738	3.801	13.062	0.984	6.059

K_S is the term for the energy of interaction with the surface, l/mmol; K_L is the equilibrium constant for surface sorption–desorption, l/mmol

and BET equations. Contrary to the Langmuir and Freundlich isotherms, which represent sorption of BSs either on homogeneous, or on heterogeneous surface of MSNs, the Redlich–Peterson model is appropriate for description of hybrid sorption process, whereas BET equation concerns multilayer sorption from the liquid phase (Gritti and Guiochon 2003; Ebadi et al. 2009). Substantial difference in R^2 values proves that neither the Langmuir no the Freundlich models can describe the experimental equilibrium sorption data correctly. At the same time, both the Redlich–Peterson

and BET models give high values of correlation coefficients. To ensure the suitability of one of these models for precise description of experimental sorption isotherms, the results of Chi-square test (χ^2) were compared (Tables 5, 6). It was found that application of the Redlich–Peterson model gives higher values of χ^2 in comparison with that ones obtained for the BET model (Tables 5, 6). Therefore, it can be concluded that an assessment of statistical error functions reveals multilayer sorption of BSs on MSNs. The isotherm curves predicted by non-linear regression analysis

Fig. 12 Isotherms of NaC (a) and NaTC (b) sorption by 1-MSN (curve 1), 2-MSN (curve 2), and 3-MSN (curve 3) from PBSs with pH 5.0 calculated using non-linear modeling of experimental results with the BET equation

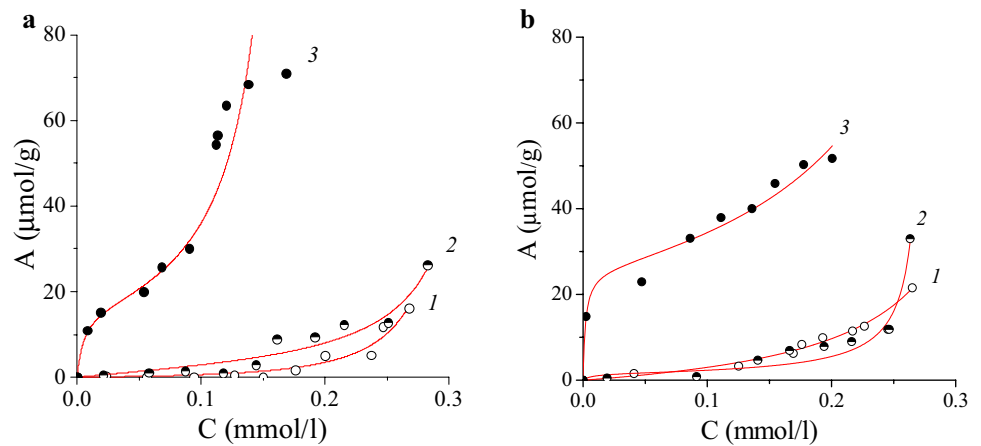
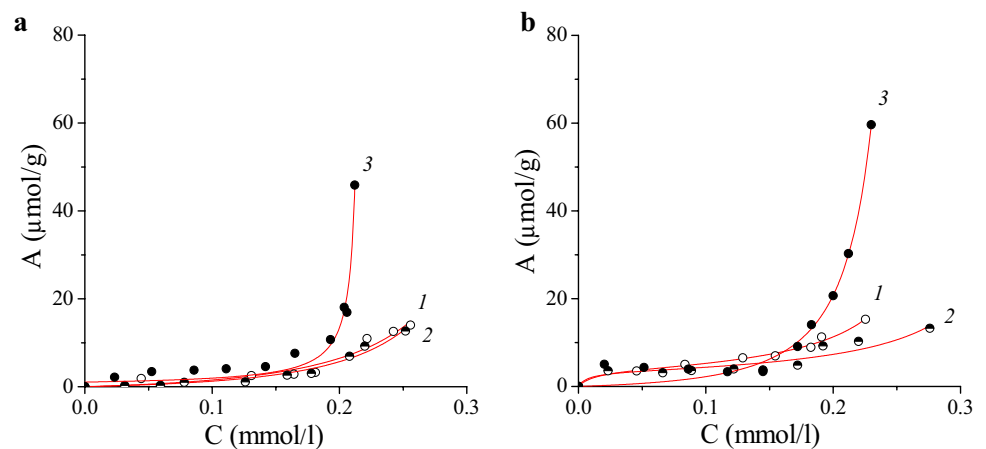


Fig. 13 Isotherms of NaC (a) and NaTC (b) sorption by 1-MSN (curve 1), 2-MSN (curve 2), and 3-MSN (curve 3) from PBSs with pH 7.4 calculated using non-linear modeling of experimental results with the BET equation



of the BET equations are close to the experimental ones (Figs. 12, 13). In all cases, sorption capacity increases in the region of high equilibrium concentrations at both studied pH values, proving cooperative mechanism of BSs sorption in studied systems. Obviously, BSs, which form the first sorption layer on MSNs surface, serve as sorption sites for the second layer, and so on.

Since sorption of BSs depends significantly on the protolytic state of adsorbate and surface groups of adsorbent, the pH of medium should be taken into account at discussion of the comparative sorption efficiency. In accordance with the obtained experimental results, sorption of NaC and NaTC from solutions with equilibrium concentration 0.2 mmol/l by 3-MSN is equal to 15 and 20 $\mu\text{mol/g}$ at pH 7.4 (Fig. 10) and increases up to 70 and 50 $\mu\text{mol/g}$, correspondingly, at pH 5.0 (Fig. 11). Obtained values are higher than reported binding capacity of aqueous enzymatic extract from rice bran for NaTC and NaDC (11 and 8 $\mu\text{mol/g}$, correspondingly) at pH 6.3 (Wang et al. 2018), cholestyramine for HCA and NaTC (11 and 19 $\mu\text{mol/g}$, correspondingly) at pH 5.0 (Kazlauske et al. 2014), and chitosan for HCA (9 $\mu\text{mol/g}$) at pH 5.0 (Kazlauske et al. 2014). The sorption capacity

of cellulose, wood powders, and individual lignins in relation to NaC varies from 4 to 28 $\mu\text{mol/g}$, whereas for enzymatically treated lignins, this value reaches 28 $\mu\text{mol/g}$ at pH 6.9 (Zuman et al. 1988). Synthesized in the present work, 3-MSN material demonstrates sorption ability commensurable with chitosan–fumed silica composite, which attains 43 and 97 $\mu\text{mol/g}$ for CA and TCA, correspondingly, at pH 4 (Budnyak et al. 2019). The binding capacity of diethylaminoethyl derivative of cellulose consists of 135 $\mu\text{mol/g}$ for HCA and 130 $\mu\text{mol/g}$ for NaTC at pH 5.0 (Kazlauske et al. 2014). It can be concluded that chemical immobilization of steroid functional groups in the surface layer of silica material possessing good biocompatibility and low toxicity opens up new possibilities for design of medical sorbents for BSs sorption removal and hypercholesterolemia treatment.

Conclusions

Mesoporous silica materials of MCM-41-type with surface 3-aminopropyl and steroid groups were prepared by sol–gel condensation of silica source (TEOS and APTES or their

mixture with CA-silane) in the presence of micelles of long-chain quaternary ammonium salt in individual state or with solubilized CA. The influence of CA as structure-directing and CA-silane as structure-forming agent on MSNs characteristics was studied by low-temperature nitrogen adsorption–desorption and X-ray diffraction analysis. It was found that introduction of bile acid or its triethoxysilyl derivative in sol–gel synthetic mixture has positive impact on formation of hexagonally ordered mesoporous structure of MCM-41-type silicas and results in increase of surface area and narrowing of pore diameters, especially for MSNs prepared with CA-silane participation. Sorption effectiveness of synthesized MSNs towards BSs was studied from PBSs in dependence of duration of contact, solution pH, and adsorbate equilibrium concentration. Due to the good availability of surface sorption centers located in tunable pore channel, all synthesized MSNs demonstrate high sorption kinetic parameters. Efficiency of BSs sorption removal by MSNs is predetermined by the protolytic state of adsorbate and adsorbent ionogenic groups, and achieves maximal values at pH ~ 5 for NaC and pH ~ 2 for NaTC. Equilibrium sorption studies prove that chemical immobilization of steroid groups results in noticeable enhancement of silica material sorption ability, especially in the region of small equilibrium concentrations at pH 5 that is not typical for MSNs with surface 3-aminopropyl groups. Analysis of experimental sorption isotherms by the Langmuir, Freundlich, Redlich–Peterson, and BET models evidences multilayer character of BSs sorption on MSNs. Silica materials with chemically immobilized steroid groups demonstrate high sorption ability towards BSs and have potential in hypercholesterolemia diagnostics and treatment.

Funding We received no funding for this study.

Declarations

Conflict of interest We have no competing interests.

Ethical approval This article does not contain any studies with human participants or animals performed by any of the authors.

References

- Asefa T, Tao Z (2012) Biocompatibility of mesoporous silica nanoparticles. *Chem Res Toxicol* 25:2265–2284
- Belyakova LA, Besarab LN (2007) The influence of the structure of the surface of hydrophilic-hydrophobic silicas on the adsorption of cholic acid. *Russ J Phys Chem A* 81:1537–1541
- Belyakova LA, Varvarin AM, Besarab LN, Vlasova NN, Golovkova LP (2005) Role of hydrophobic interactions in the adsorption of cholic acids at silicas. *Russ J Phys Chem A* 79:518–522
- Belyakova LA, Besarab LN, Roik NV, Lyashenko DY, Vlasova NN, Golovkova LP, Chuiko AA (2006) Designing of the centers for adsorption of bile acids on a silica surface. *J Colloid Interface Sci* 294:11–20
- Bergheanu SC, Bodde MC, Jukema JW (2017) Pathophysiology and treatment of atherosclerosis. Current view and future perspective on lipoprotein modification treatment. *Neth Heart J* 25:231–242
- Bloch CA, Watkins JB (1978) Determination of conjugated bile acids in human bile and duodenal fluid by reverse-phase high-performance liquid chromatography. *Lipid Res* 19:510–513
- Bragg WL (1913) The diffraction of short electromagnetic waves by a crystal. *P Camb Philos Soc* 17:43–57
- Brunauer S, Emmet PH, Teller E (1938) Adsorption of gases in multimolecular layers. *J Am Chem Soc* 60:309–319
- Budnyak TM, Vlasova NN, Golovkova LP, Slabon A, Tertykh VA (2019) Bile acids adsorption by chitosan-fumed silica enterosorbent. *Colloid Interface Sci Comm* 32:100194
- Carey MC, Small DM (1972) Micelle formation by bile salts. Physical-chemical and thermodynamic considerations. *Arch Intern Med* 130:506–527
- Cashin-Hemphill L, Mack WJ, Pogoda JM, Sanmarco ME, Azen SP, Blankenhorn DH (1991) Beneficial effects of colestipol-niacin on coronary atherosclerosis. A 4-year follow-up. *JAMA* 264:3013–3017
- Chen J, Han W, Chen J, Zong W, Wang W, Wang Y, Cheng G, Li C, Ou L, Yu Y (2017) High performance of a unique mesoporous polystyrene-based adsorbent for blood purification. *Regen Biomater* 4:31–37
- Clas SD (1991) Increasing the in vitro bile acid binding capacity of diethylaminoethylcellulose by quaternization. *J Pharm Sci* 80:891–894
- Dawson PA, Karpen SJ (2015) Intestinal transport and metabolism of bile acids. *J Lipid Res* 56:1085–1099
- Ebadi A, Mohammadzadeh JSS, Khudiev A (2009) What is correct form of BET isotherm for modeling liquid phase adsorption? *Adsorption* 15:65–73
- Evans DF, Pye G, Bramley R, Clark AG, Dyson TJ, Hardcastle JD (1988) Measurement of gastrointestinal pH profiles in normal ambulant human subjects. *Gut* 29:1035–1041
- Fenelonov VB, Romannikov VN, Derevyankin AYU (1999) Mesopore size and surface area calculations for hexagonal mesophases (types MCM-41, FSM-16, etc.) using low-angle XRD and adsorption data. *Micropor Mesopor Mater* 28:57–72
- Goto J, Hasegawa M, Kato H, Nambara T (1978) A new method for simultaneous determination of bile acids in human bile without hydrolysis. *Clin Chim Acta* 87:141–147
- Gregg SH, Sing KS (1913) Adsorption, surface area and porosity. Academic Press, New York
- Gritti F, Guiochon G (2003) New thermodynamically consistent competitive adsorption isotherm in RPLC. *J Coll Int Sci* 264:43–59
- Grun M, Unger KK, Matsumoto A, Tsutsumi K (1997) Ordered mesoporous MCM-41 adsorbents: novel routes in synthesis, product characterization and specification. Royal Society of Chemistry, Great Britain, Characterisation of Porous Solids IV
- Hageman J, Herrema H, Groen AK, Kuipers F (2010) A role of the bile salt receptor FXR in atherosclerosis. *Arterioscler Thromb Vasc Biol* 30:1519–1528
- Haratake M, Ogawa N, Sugii A (1989) Sorption characteristics of anion-exchange resins possessing w-oxoalkyl or w-hydroxyalkyl spacer for bile acids. *Anal Sci* 5:687–690
- Hofmann AF (2009) The enterohepatic circulation of bile acids in mammals: form and functions. *Front Biosci (landmark Ed)* 4:2584–2598
- Insull W (2006) Clinical utility of bile acid sequestrants in the treatment of dyslipidemia: a scientific review. *South Med J* 99:257–273

- Jaganathan H, Godin B (2012) Biocompatibility assessment of Si-based nano- and micro-particles. *Adv Drug Deliv Rev* 64:1800–1819
- Jana PK, Moulik SP (1991) Interaction of bile salts with hexadecyltrimethylammonium bromide and sodium dodecyl sulfate. *J Phys Chem* 95:9525–9532
- Kazlauske J, Ramanauskienė K, Liesienė J (2014) Binding of bile acids by cellulose-based cationic adsorbents. *Cellul Chem Technol* 48:11–17
- Krasopoulos JC, De Bari VA, Needle MA (1980) The adsorption of bile salts on activated carbon. *Lipids* 15:365–370
- Kruk M, Jaroniec M, Sayari A (1997) Adsorption study of surface and structural properties of MCM-41 materials of different pore sizes. *J Phys Chem B* 101:583–589
- Lai W, Yang S, Jiang Y, Zhao F, Li Z, Zaman B, Fayaz M, Li X, Chen Y (2020) Artefact peaks of pore size distributions caused by unclosed sorption isotherm and tensile strength effect. *Adsorption* 26:633–644
- Landers J, Gor GYu, Neimark AV (2013) Density functional theory methods for characterization of porous materials. *Colloid Surf A* 437:3–32
- Meissner M, Wolters H, de Boer RA, Havinga R, Boverhof R, Bloks VW, Kuipers F, Groen AK (2013) Bile acid sequestration normalizes plasma cholesterol and reduces atherosclerosis in hypercholesterolemic mice. No additional effect of physical activity. *Atherosclerosis* 28(1):117–123
- Neimark AV, Ravikovitch PI, Grun M, Schuth F, Unger KK (1998) Pore size analysis of MCM-41 type adsorbents by means of nitrogen and argon adsorption. *J Coll Int Sci* 207:159–169
- Nichifor M, Zhu X, Baille W, Cristea D, Carpov A (2001) Bile acid sequestrants based on cationic dextran hydrogel microspheres. 2. Influence of the length of alkyl substituents at the amino groups of the sorbents on the sorption of bile salts. *J Pharm Sci* 90:681–689
- Padasala S, Patel V, Ray D, Singh K, Aswal VK, Bahadur P (2016) Bile salt assisted morphological changes of cationic gemini surfactant (12-4-12) micelles. *RSC Adv* 6:96584–96594
- Raedsch R, Hofmann AF, Tserng K-Y (1979) Separation of individual sulfated bile acid conjugates as calcium complexes using reversed-phase partition thin-layer chromatography. *J Lipid Res* 20:796–800
- Reddy BS, Watanabe K, Sheinfil A (1980) Effect of dietary wheat bran, alfalfa, pectin and carrageenan on plasma cholesterol and fecal bile acid and neutral sterol excretion in rats. *J Nutr* 110:1247–1254
- Reiner Z, Catapano AL, De Backer G, Graham I, Taskinen M-R, Wiklund O, Agewall S, Alegria E, Chapman MJ, Durrington P, Erdine S, Halcox J, Hobbs R, Kjekshus J, Filardi PP, Riccardi G, Storey RF, Wood D (2011) ESC/EAS Guidelines for the management of dyslipidaemias: the Task Force for the management of dyslipidaemias of the European Society of Cardiology (ESC) and European Atherosclerosis Society (EAS). Developed with the special contribution of the European Association for Cardiovascular Prevention and Rehabilitation (EACPR). *Eur Heart J* 32:1769–1818
- Ripatti PO, Popova RA, Kagan TB, Bekhtereva ZA (1969) Spectrophotometric determination of bile acids. *Vopr Med Khim* 15:630–633 (In Russian)
- Roda A, Hofmann AF, Mysels KJ (1983) The influence of bile salt structure on self-association in aqueous solution. *J Biol Chem* 258:6362–6370
- Sasaki Y, Miyassu Y-I, Lee S, Nagadome S, Igimi H, Sugihara G (1996) The adsorption behavior of four bile salt species on activated carbon in water at 30°C. *Colloids Surf B* 7:181–188
- Shen J, Yang X, Sun X, Gong W, Ma Y, Liu L, Yao J (2020) Amino-functionalized cellulose: a novel and high-efficiency scavenger for sodium cholate sorption. *Cellulose* 7:14019–14028
- Strand J, Lewis R, Wissman C, Carr S (2012) Synthesis and characterization of selective mesoporous sol-gel silica sorbent for detection of estrone in wastewater via molecularly imprinted solid phase extraction. *Int J Separ for Environ Sci* 1:37–54
- Sun L, Duan R, Fan Y, Chen X-Z, Peng C, Zheng C, Dong L-Y, Wang X-H (2020) Preparation of magnetic mesoporous epoxy resin by initiator-freeing-opening polymerization for extraction of bile acids from humanserum. *J Chromatogr A* 1609:460448–460458
- Swanson-Vethamuthu M, Almgren M, Hansson P, Zhao J (1996) Surface tension studies of cetyltrimethylammonium bromide–bile salt association. *Langmuir* 12:2186–2189
- Thommes M, Smarsly B, Groenewolt M, Ravikovitch PI, Neimark AV (2006) Adsorption hysteresis of nitrogen and argon in pore networks and characterization of novel micro- and mesoporous silicas. *Langmuir* 22:756–764
- Van Der Voort P, Ravikovitch PI, De Jong KP, Benjelloun M, Van Bavel E, Janssen AH, Neimark AV, Weckhuysen BM, Vansant EF (2002) A new templated ordered structure with combined micro- and mesopores and internal silica nanocapsules. *J Phys Chem B* 106:5873–5877
- Wang Y, Yu G, Zang X, Ye F (2018) Optimization, antioxidant activity and bile salts adsorption capacity of the aqueous enzymatic extract from rice bran. *Czech J Food Sci* 36:338–348
- Watkins JB, Klaassen CD (2010) Absorption, enterohepatic circulation, and fecal excretion of toxicant. In: McQueen CA (ed) *Comprehensive toxicology*. Elsevier, Oxford, pp 77–91
- Watts GF, Lewis B, Lewis ES, Coltart DJ, Smith LDR, Swan AV, Brunt JNH, Mann JI (1992) Effects on coronary artery disease of lipid-lowering diet, or diet plus cholestyramine, in the St Thomas' Atherosclerosis Regression Study (STARS). *Lancet* 339:563–569
- Yi R, Song Y, Wu C, Wei G, Yuan R, Chen Y, Ye G, Kowalewski T, Matyjaszewski K (2020) Preparation of nitrogen-doped mesoporous carbon for the efficient removal of bilirubin in hemoperfusion. *ACS Appl Bio Mater* 3:1036–1043
- Zhu X, Wen Y, Wang L, Li C, Cheng D, Zhang H, Ni Y (2014) Binding of sodium cholate in-vitro by cationic microfibrillated cellulose. *Ind Eng Chem Res* 53:18508–18513
- Zuman P, Ainsworth S, Paden C, Pethica BA (1988) Sorption on lignin, wood and celluloses. I Bile Salts *Colloids Surf A* 33:121–132

Publisher's Note Springer Nature remains neutral with regard to jurisdictional claims in published maps and institutional affiliations.

Springer Nature or its licensor (e.g. a society or other partner) holds exclusive rights to this article under a publishing agreement with the author(s) or other rightsholder(s); author self-archiving of the accepted manuscript version of this article is solely governed by the terms of such publishing agreement and applicable law.